RSC Advances

PAPER

View Article Online
View Journal | View Issue

Cite this: *RSC Adv.*, 2025, **15**, 40328

Enhanced microstructure as well as mechanical and oxidation resistance of C/C–SiC composites fabricated by RMI for thermal protection

Yanli Huo,[a] Yufeng Chen,[a] Shouwan Qin,[b] Hailin Liu,[a] Hailong Liang,[a] Jiajia Ma,[a] Haoran Sun[a] and Xiankai Sun *[a]

In this study, two-dimensional needle-punched laminated C fibres were used as preforms, and interfacial phases were prepared *via* chemical vapor infiltration (CVI) using pyrolytic carbon (CVI-PyC), sucrose-derived carbon (S/C), and pitch-derived carbon (P/C). The effects of interfacial phases on fibre coatings and siliconizing properties were investigated. The results demonstrated that the CVI-PyC interfacial phase is the most continuous and dense, providing the best protection effect on the fibres and forming a uniform cylindrical structure after siliconizing. The S/C interfacial phase is the second best; however, the matrix is fragmented after siliconizing. The P/C interfacial phase is the worst, leading to a lamellar surface structure and microcracks after siliconizing. Using CVI-PyC and S/C alternately as matrix carbon sources, C/C–SiC composites were synthesized *via* reactive melt infiltration, which comprised carbon fibres, SiC, and residual Si. According to mechanical property test results, the bending and tensile strengths of the prepared C/C–SiC composites were 345.4 and 156 MPa, respectively, which are considerably higher than those of single sucrose-derived carbon (134 and 75 MPa, respectively) and CVI-PyC matrix carbon (261.9 and 108 MPa, respectively). Oxidation-resistant coatings were prepared on the surface of the materials through chemical vapor deposition. High-temperature examination demonstrated that the coating effectively inhibited fibre oxidation, and the tensile strength retention rate reached 41% at 1500 °C in an oxygen environment, whereas the strength of the uncoated samples decreased to <10 MPa. This study provides an important reference for optimizing the interface design and high-temperature oxidation resistance of C/C–SiC composites.

Received 6th July 2025
Accepted 9th September 2025

DOI: 10.1039/d5ra04829j

rsc.li/rsc-advances

1 Introduction

With the intensive development of lunar exploration projects and the increasingly frequent round-trip missions between Earth and the moon, the demand for research and development of aerospace vehicles has become increasingly urgent. During repeated atmospheric crossings, the hot-end components of the aircraft are subjected to complex alternating loads, extreme temperatures, and harsh thermophysical and chemical environments. Thus, a reliable thermal protection system is required to guarantee the performance of the aircraft. Continuous fibre-reinforced ceramic matrix composites have become ideal thermal structural materials owing to their excellent high-temperature and mechanical properties. Among these composites, carbon fibre–reinforced silicon carbide (C/C–SiC) composites[1,2] are stable in high-temperature environments without additional thermal protection because of their high specific strength, good fracture toughness, fatigue resistance, and excellent creep resistance, which can remarkably reduce structural weight and improve reusability.[3–6]

At present, the primary methods for preparing C/C–SiC composites are chemical vapor infiltration (CVI), powder/slurry hot pressing, precursor cracking (PIP), and reactive melt infiltration (RMI). Among these, materials prepared using the PIP and CVI methods exhibit stable properties; however, they are time-consuming, and their equipment requirements are high. Thus, their high preparation cost limits their extensive applications in civil fields.[7–10] The powder/slurry hot pressing method is less time consuming. However, it has high equipment requirements and can only prepare products with simple shapes. Therefore, this method is not suitable for civil fields.[11,12] The RMI method has the advantages of a short preparation period, low residual porosity, and the ability to prepare workpieces with a net size and complex shape. Therefore, it is termed as a reliable method for preparing C/C–SiC composites at low cost.[13–15] However, owing to the influence of carbon fibre quality, preform and interfacial phase structure, matrix carbon structure, density, pore size and distribution, and process parameters of RMI, the properties of RMI-prepared C/C–SiC composites differ.

[a]*China Building Materials Academy, Beijing 100024, China. E-mail: sunxiankai2008@163.com*

[b]*School of Civil Engineering and Architecture, Henan University of Technology, Zhengzhou 450001, China*

Herein, two-dimensional (2D) needle-punched laminated carbon fibres were used as preforms, and pyrolytic carbon (PyC) was deposited as the interfacial phase *via* CVI.[16,17] For comparison, interfacial phases were prepared using sucrose-derived PyC (S/C)[18,19] and pitch-derived carbon (P/C).[20,21] The microstructural characteristics of the three interfacial phases were systematically compared, and their effects on fibre coating and siliconizing properties were investigated. C/C–SiC composites were prepared *via* RMI by siliconizing C/C preforms with different carbon source structures, and their microstructures, mechanical properties, and oxidation resistance were analyzed. Moreover, an oxidation-resistant coating was prepared on the material surface *via* chemical vapor deposition (CVD), and the influencing mechanism of the coating on the high-temperature mechanical properties of the material was explored. This study provides an important basis for optimizing the interface design and high-temperature oxidation resistance of C/C–SiC composites.

2 Experimental

A schematic of the preparation process is shown in Fig. 1. In total, there are 3 steps in the procedure for C/C–SiC composite preparation; *i.e.*, the interface phase preparation, carbon matrices preparation, and siliconizing process. Three different methods in Sections 2.1 to 2.3 were employed to prepare the interface phase to form the C/C preform. The same methods could be used to prepare the carbon matrices as long as the original carbon fabric was replaced by the C/C preform. The siliconizing process was the reaction between the melted Si and the carbon matrices at 1500 °C in a vacuum.

2.1 Preparation of the interface phase by CVI-PyC

The 12K needle-punched laminated carbon fiber preforms were purchased from Zhong Fu Shen Ying Carbon Fibre Co., Ltd. The above carbon fabric with a density of 0.65 g cm^{-3} and a thickness of 6 mm was used. The method for preparing the interface phase *via* CVI involved using propane as the precursor gas and nitrogen as the carrier gas, with a propane-to-nitrogen molar ratio of 1 : 5. Propane at a flow rate of 2 L min^{-1} was introduced into a pyrolysis furnace with a nitrogen atmosphere at a pressure of 4 kPa. The furnace chamber, cylindrical in shape with a diameter of 1200 mm and a height of 900 mm, was maintained at a temperature of 900 °C. Deposition was carried out for 1 hour to prepare the CVI-PyC interface.

2.2 Preparation of the interface phase by S/C

The carbon fibre fabric was immersed in a 0.5 mol L^{-1} $FeCl_3 \cdot 6H_2O$ solution for 12 hours to ensure uniform attachment of $FeCl_3$ (catalyst) on the carbon fibre surface. A 70 wt% solution was prepared by mixing sucrose, acrylamide, and *N*,*N*′-methylenebisacrylamide, followed by the addition of an initiator. The carbon fibre fabric was further immersed in these 70 wt% sucrose-monomer solutions for 10 minutes. The system was evacuated to −0.1 MPa, and the fibre preform was immersed in the solution under vacuum (−0.1 MPa) for 5 minutes. After restoring atmospheric pressure, a gas pressure of 3 MPa was applied in a pressure impregnation device to fully infiltrate the sucrose solution into the fabric. The impregnated preform was placed in a reaction kettle and heated in an oven at 80 °C for 1 hour to allow sucrose infiltration and solidification within the preform. The preform was then removed, and any sucrose gel adhering to the surface was cleaned off. It was subsequently transferred to an oven for pre-carbonization at 300 °C for 3 hours, followed by pyrolysis in a vacuum furnace at 1100 °C to form glassy carbon. Finally, it was carbonized at 1800 °C to form S/C attached to the fibre surface.

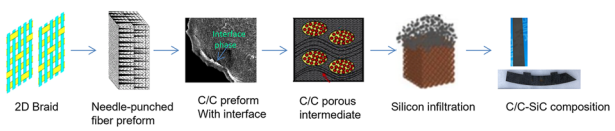

Fig. 1 Schematic flow chart of the C/C–SiC composite preparation *via* RMI.

2.3 Preparation of the interface phase by alternating S/C and CVI-PyC

The sucrose-monomer solution prepared in Section 2.2 was also used in this section. First, the fibre preform with the PyC carbon interfacial phase was immersed in the solution for two cycles of impregnation-curing-pyrolysis. Subsequently, CVI infiltration of PyC was performed for 50 hours, followed by two cycles of impregnation at 3 MPa pressure and pyrolysis at 1100 °C. CVI carbon infiltration was conducted for another 50 hours to achieve a density of approximately 1.4 g cm^{-3} for the C/C preform.

2.4 Characterization

The microstructures of the materials were analyzed using field-emission scanning electron microscopy (SEM; accelerating voltage: 200 V–30 KV; FEI Company Quanta 250 FEG). The composite composition was analyzed using X-ray diffraction (XRD; D8 Advance X-ray diffractometer with a power rating of 18 kW; Germany Brooks Company).

Tensile properties were investigated using a high-temperature electronic universal testing machine (Instron 3369), and the displacement loading mode was adopted at a loading rate of 1 mm min^{-1}. The size of the tensile specimen at ambient temperature (22–25 °C) was 120 mm × 10 mm × 3 mm, and the tensile specimen under high-temperature air atmosphere was dumbbell-shaped, as shown in Fig. 2.

The bending performance of the C/C–SiC composites was tested using a microcomputer-controlled electronic universal

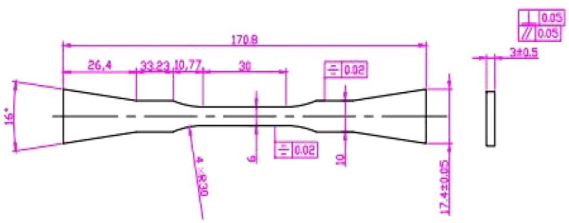

Fig. 2 Tensile specimen size under a high-temperature air atmosphere.

testing machine (MTS C 45.105). The sample was cut into 3 mm × 4 mm × 36 mm test strips, and the bending strengths of the carbon fibre-toughened ceramic matrix composites at ambient temperature were evaluated using the three-point bending method. The strength value σ was calculated as follows:

$$\sigma = \frac{3P_f L}{2wh^2} \quad (1)$$

where P_f denotes the fracture load of the composite material (n), L represents the style span (mm); w represents the style width (mm), and h represents the style height (mm).

3 Results and discussion

3.1 The effects of carbon sources with different preparation processes on interfacial phase microstructure

Before preparing continuous fibre-reinforced SiC matrix composites *via* RMI, the first problem to be analyzed and solved is the suppression of carbon fibre damage. To avoid high-temperature silicon vapor eroding the C fibre, it is typically necessary to prepare an interfacial phase on the surface of the C fibre, which is generally combined with the fibre and matrix. When the composites are damaged, the fibres are pulled out to strengthen and toughen them to avoid catastrophic damage.[22,23] The interfacial phase improves some properties of the carbon fibre surface, facilitates the realization of appropriate interfacial bonding energy, and enhances the toughness of composite materials. Furthermore, the phase can prevent fibre erosion and damage by silicon vapor during RMI.

Herein, S/C, P/C, and CVI-prepared PyC were used to prepare interfacial phases to protect carbon fibres. The effects of the phase–fibre–matrix structure and the interfacial phase on the mechanical properties of the prepared composites were analyzed.

The sucrose pyrolysis process is divided into two steps: initially, glucose and fructose are formed, and then further dehydration and polycondensation are conducted to form small molecular polymers. Among these polymers, 5-hydroxymethylfurfural is the most important intermediate product, which tends to polymerize to form a carbon structure.[24–26]

$$C_{12}H_{22}O_{11} \rightarrow 12C + 11H_2O \quad (2)$$

Owing to the adhesion of high sugar concentrations, the sucrose solution adheres to the fibre surface, whereas the sugar in the pores can discharge through extrusion. The SEM images after pyrolysis at high temperatures show that the sucrose solution thoroughly infiltrates the C fibre preform, and the carbon after sucrose pyrolysis is close to the fibre surface and piled up on the fibre surface in a granular form, thus making the fibre surface rough. Some particles are fused and connected into sheets, which have a good coating effect on the fibre and are closely combined with the C fibre; however, as shown in Fig. 3a, the particles are not completely continuous.

Pitch primarily contains heavy aromatics and polycyclic naphthalene, and its cracked carbon yield is high.[27] In this experiment, the pitch was placed in an 80 °C vacuum oven until it melted. The fibre preform was then immersed in the molten pitch, and a vacuum was applied to ensure that the pitch fully impregnated the preform. The experimental results revealed that the pitch pyrolysis product (P/C) exhibited less attachment to the fibre surfaces. Instead, it predominantly filled the spaces between fibre bundles, forming discontinuous flake-like distributions among the fibre tows.

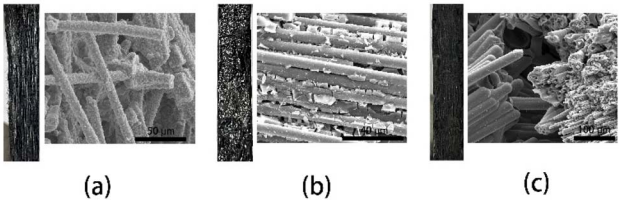

Fig. 3 The photo images and morphology of pyrolytic carbon-coated C fibres: (a) sucrose-derived pyrolytic carbon; (b) pitch-derived pyrolytic carbon; and (c) propane-based CVI-prepared pyrolytic carbon.

The PyC sample pyrolyzed by propane-based CVI was in a continuous and dense state, and the sample was tightly wrapped with carbon fibres. The S/C and CVI-PyC samples exhibited better coating properties on the carbon fibres than the asphalt-derived pyrolytic P/C samples. Fig. 3 shows the morphologies of the primary pyrolysis of different precursors.

The SEM results demonstrated that the carbon prepared by S/C and CVI-PyC adhered to the fibre surface, as shown by Fig. 3a and c. The pyrolytic carbon was coated onto the fibre surface, whereas the pitch-derived carbon was mostly located between fibre bundles and grew in discontinuous layers. When compared with CVI-PyC, the carbon on the fibre surface of the sucrose-and pitch-derived PyC samples was looser and even more disordered. The carbon coating on the fibre surface seemed rough and discontinuous, and was unable to form a dense barrier. This is mainly because pitch and sucrose shrink in volume during drying and pyrolysis; thus, complete carbon cannot be formed. Different from sucrose- and pitch-derived PyC, CVI-prepared PyC piles up in sheet-like folds, and its lamellae are parallel to the axial direction of the fibre, forming a concentric PyC layer. This layer keeps growing around the fibre surface and evenly covers the fibre surface. CVI is more suitable for preparing the interfacial phase because the produced carbon tightly wraps the fibre to form a protective barrier.

The weight of the carbon fibre preform used in the experiment was 25 g, and the weight gains of PyC after 1 h of carbon deposition *via* CVI deposition and soaking in sucrose and asphalt solutions were 5.4, 5.2, and 5.3 g, respectively. As shown by Fig. 4, the weight gains for the three samples are close to each other; *i.e.*, the amounts of carbon generated are similar. Comparisons of the three types of carbon matrices were made, and investigations were conducted as presented in the following sections.

3.2 Analysis of the microscopic properties of carbon matrices produced by three different methods

The above experiments have demonstrated that sucrose solutions can effectively soak the fibre, and the carbon particles generated by sucrose pyrolysis can effectively attach to the fibre

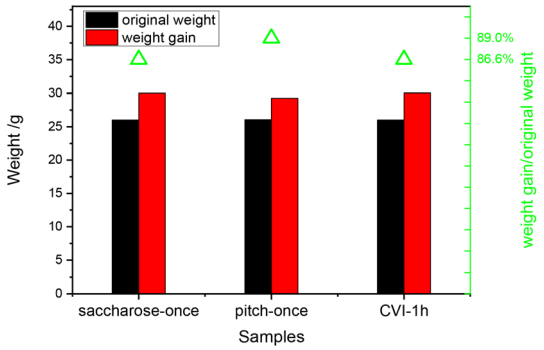

Fig. 4 Weight gain of knitted fabrics for three different treatment methods.

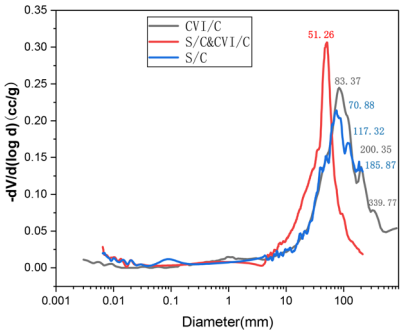

Fig. 6 Pore size distribution of materials after three types of carburizing (gray represents CVI/C, red represents S/C&CVI/C alternation, and blue represents S/C).

surface. Therefore, we attempted to densify the fibre preform containing the PyC interfacial phase using a sucrose monomer polymerization solution, combined with repeated impregnation–pyrolysis processes. The specific operation was as follows: sucrose (Fig. 5a) was retained in the preform by monomer initiation curing, and precarbonization was then performed at 300 °C. However, at 300 °C, sucrose was carbonized and contracted, forming a continuous dense aggregate (Fig. 5b), which made the subsequent impregnation difficult. To overcome this challenge, the preform was treated at 1100 °C to carbonize the aggregate, and the sucrose solution was then subjected to secondary impregnation and carbonization densification. The experimental results demonstrated that the sucrose solution penetrated the preform smoothly during the first impregnation and the aggregate structure changed after high-temperature treatment, thus forming a sponge-like porous carbon after sucrose pyrolysis (Fig. 5c). This porous structure considerably improved the penetrability of the sucrose solution, which is highly beneficial for the further infiltration and densification of the sucrose solution into the preform.

After protecting the carbon fibre, it is necessary to further prepare the C matrix so that it can react with Si and form the SiC matrix. If the C matrix is too loose, it cannot prevent silicon from eroding the fibre; while, if the C matrix is too dense, it is not conducive to the infiltration of molten silicon. Ran Liping *et al.*[28] reported that the protection of carbon fibre is necessary to form SiC highly efficiently by RMI. In this study, the formation of the preforms also plays a decisive role in the carbon matrices and the following siliconization. In particular, the density and porosity[29] of the preforms and the carbon matrices are critical parameters that influence the mechanical and thermal resistance of the final C/C–SiC composites.

Fig. 5 Pre-carbonization and post-carbonization morphology of sucrose gel.

Herein, the porosity and pore size of the C/C preforms prepared by S/C, CVI/C, and S/C&CVI/C alternation were analyzed, as shown in Fig. 6. The densities of these preforms are the same, *ca.* 1.4 g cm^{-3}. The pore size distributions of the composites prepared by CVI/C are broad. The minimum pore size of CVI/C is 83.37 μm, and the maximum pore size is 339.77 μm. During the densification of fibre preforms using the CVI process, gas diffusion within the pores of the fibre bundles initially follows Fick diffusion (molecular diffusion), while in the later stages, Knudsen diffusion becomes dominant.[30,31] The pore structure is primarily determined by the balance between gas accessibility and deposition rate. Small-sized pores may be preferentially filled with deposited carbon due to their larger specific surface area, whereas large-sized pores are prone to forming surface-sealed pores due to gas diffusion limitations. Additionally, the excessive deposition of reactive gases on the outer surface of the preform forms a dense layer, which hinders internal gas diffusion and results in density inhomogeneity.

Compared with CVI, sucrose-derived carbon typically exhibits a hierarchical pore size distribution. The smallest and largest pore sizes are 70.88 and 185.87 μm, respectively. Sucrose aqueous solution can penetrate the smallest pores through capillary action, leading to its pyrolytic carbon filling the inter-fibre spaces, as seen in Fig. 3. The pores in carbon derived from sucrose infiltration primarily originate from pyrolysis volatilization and volume shrinkage. During the sucrose pyrolysis process, the escape of gaseous products tends to form an interconnected pore network, which can provide pathways for gases during chemical vapor infiltration (CVI) pyrolysis.

Therefore, the pore size distribution of the preform produced by CVI-PyC and S/C alternation is relatively uniform, and the most probable pore size distribution is approximately 51.26 μm, which is beneficial for uniform siliconization, thereby forming a uniform C/C–SiC composite structure. A difference in pore size leads to uneven siliconization, and an excessive pore size may even lead to residual silicon tumors.

Fig. 7 shows the SEM images of the three types of carburized composite materials after siliconizing. The micromorphology in Fig. 7a–c shows that the silicon carbide produced after siliconizing only with sucrose-pyrolysis carbon as the matrix is distributed discontinuously and fills the middle of fibre

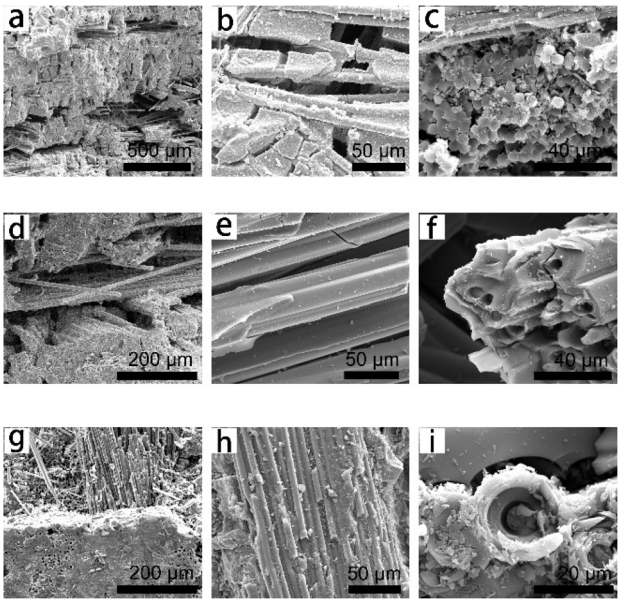

Fig. 7 Surface and cross-sectional morphologies of the three types of carburized composite materials after siliconizing. (a–c) S/C; (d–f) CVI-PyC; (g–i) S/C&CVI/C alternation.

bundles, with large pores in the materials and many cracks in the materials. In addition, the bending strength of the materials is very low, and brittle fracture occurs when they break. In contrast, the SiC produced by the melt siliconizing reaction of the CVI-PyC composite still wraps the fibres in a tubular shape, and the SiC surface is dense and smooth, as shown by Fig. 7d–f; however, large unfilled holes are observed in the middle of the fibre bundle. The SiC composites produced after siliconizing the matrix that were alternately carburized by S/C and CVI-PyC were comparatively denser (Fig. 7g–i).

3.3 Mechanism and properties of C/C–SiC composites

3.3.1 Mechanism of silicon infiltration into carbon matrices. The most important factor affecting the RMI process is the infiltration temperature. The infiltration temperature must ensure that the infiltrator can be fully melted, and it also directly affects melt fluidity and surface tension. At a certain temperature, the silicon powder outside the C/C porous body melts, and the liquid Si penetrates the porous body along the micropores and microcracks, driven by capillary forces, and reacts with the contacted C (including carbon fibre and matrix carbon) to generate the SiC matrix. In general, the penetration depth of the melt into the pore size of the matrix can be obtained as follows:[32]

$$h = \sqrt{\frac{C\sigma\cos\theta}{2\mu}\left(r_0 t - \frac{2}{3}A_\delta t^{3/2}\right)} \quad (3)$$

where h represents the infiltration depth, C represents a constant, σ denotes the surface tension of the melt, θ denotes the wetting angle between the melt and the matrix, μ denotes the melt viscosity, r_0 denotes the initial capillary radius, t denotes the infiltration time, and A_δ denotes the temperature-determined coefficient. According to eqn (3), the factors that affect the infiltration depth include the infiltration time, melt viscosity, melt surface tension, and wetting angle between the melt and matrix. Except for the time and initial capillary radius, the other parameters are all temperature dependent. Therefore, the theoretical infiltration depth is a function of the infiltration temperature at a constant infiltration time.

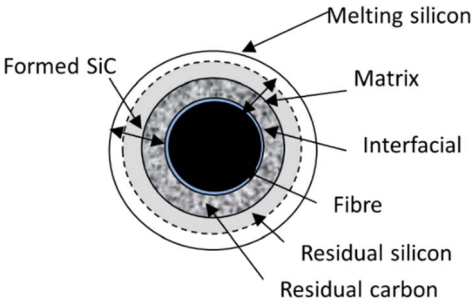

Fig. 8 Structural diagram of the siliconizing principle.

Under vacuum conditions, the formed carbon matrices were siliconized at a temperature of 1550 °C. Fig. 8 illustrates the siliconizing principle. The molten silicon infiltrated the composite surface and then its interior by capillary action. The molten silicon reacted with the matrix carbon to generate SiC. The reaction of the molten silicon weakened with increasing thickness, and the interior of the composite contained some residual C. The surface pores may be filled with residual Si.[33]

The interfacial phase acts as a bridge between the fibres and matrix, which plays a key role in load transfer, crack deflection, and fibre protection, as shown in Fig. 9. In this study, the interfacial phase somehow decides how the carbon matrix works with the melting Si.

The chemical reaction between molten Si and matrix C is as follows:

$$\mathrm{Si(l) + C(s)–SiC(s)} \quad (4)$$

The reaction between the C/C composites and Si is controlled by different mechanisms at different stages. In the initial stage, the reaction occurs at the interface between solid C and liquid Si, and the dissolution and precipitation mechanism controls the growth of SiC. The growth rate is proportional to the reaction time. When a continuous SiC layer is formed on the

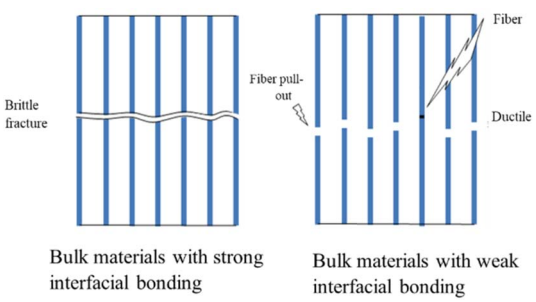

Fig. 9 Schematic of the action mechanism of the interfacial phase.

surface of solid C, the reaction occurs at the SiC/Si interface, and the reaction rate is controlled by the diffusion rate of C in the SiC layer. Thus, the formation rate of SiC decreases. In addition, the reaction between Si and C is a strong exothermic reaction, with the amount of heat released being as high as 68 kJ mol^{-1}, and volume expansion can easily cause local temperature increases and temperature gradients in the material, generating stress.

3.3.2 Morphology and properties of C/C–SiC composites. The mechanical properties of C/C–SiC composites are listed in Table 1.

As shown in Table 1, the density of the C/C–SiC composite formed by melt siliconizing with CVI-PyC as the carbon source alone is lower than that of the C/C–SiC composite formed by melt siliconizing with S/C as the carbon source alone. The carbon from CVI could form a dense, continuous coating layer on the fibre surface. The coating covers the carbon fibre, reduces the pore size, and acts as an effective barrier against silicon vapor erosion. Also, the coatings hinder the infiltration of molten silicon, resulting in the SiC formed by the reaction between molten silicon and surface PyC being very dense, while the high-density SiC hinders the further infiltration of molten silicon. Therefore, the total amount of formed SiC is too low, leading to a low density of the C/C–SiC composite. For the carbon matrix infiltrated only by S/C, its porous structure in the green body and the volume shrinkage during sucrose carbonization cause a loose bonding state between the carbon matrix and fibre. The gap in the middle allows for the full infiltration of silicon and the full reaction of C in the S/C green body, leading to the generation of SiC and less residual silicon. The residual silicon usually fills the macropores and voids of SiC. The porosity plays an important role in forming SiC. The lower the porosity, the more SiC is generated and the less residual Si. As shown by Table 1, when comparing the three carbon matrices after RMI, the bending strength is the greatest when the porosity is the least. Owing to the porous structure of sucrose-derived carbon, the SiC particles generated by the new reaction are loosely filled between fibre bundles, which cannot form a dense and continuous structure. Both the loose SiC and the discontinuity of matrix carbon facilitate Si to penetrate through cracks and contact the surface of the carbon fibre and locally react to damage the carbon fibre. The above factors account for its low bending strength.

Based on the above considerations, an optimal method using alternative S/C and CVI-PyC was employed to prepare the carbon matrix. In such a case, the carbon matrix includes a suitable amount of pores with a narrow size distribution, so that the silicon can fully react with carbon to form SiC, which can reduce the amount of residual Si after reaction infiltration. The smaller the amount of the residual Si, the better the mechanical performance of the C/C–SiC composites. As listed in Table 1, the outstanding bending strength of 345.4 MPa and tensile strength of 156.0 MPa were observed for the carbon matrix with alternating S/C and CVI-PyC after RMI. The results indicate that the method of alternating S/C and CVI-PyC used in this work is very effective in improving the microstructure and mechanical performances of the carbon matrix as well as the C/C–SiC composites.

Alternate treatments with S/C and CVI-PyC caused the density of the preform to reach approximately 1.4 g cm^{-3}, and then the siliconizing treatment was performed. At high temperatures, molten silicon enters the fibre gap or the micropore channel of the treated preforms *via* capillary force and reacts with the contact C to form SiC. During this process, high-density carbon fibre–reinforced SiC matrix composites can be obtained while protecting the C fibres to avoid performance degradation owing to silicification. PyC prepared by CVI pyrolysis is used as the interfacial phase. Fig. 9 shows the morphology of the C/C preform densified by alternating sucrose pyrolysis and CVI after siliconizing. The C fibre is located in the middle, and a gap between the C fibre and the SiC phase is generated by the reaction owing to the difference in the thermal expansion coefficient.

3.3.3 Oxidation analysis of fibre composites after siliconizing the alternately carburized matrix. Fig. 10 shows the fracture morphology of the composite material at ambient temperature and 1500 °C in air, respectively. After the tensile fracture of the composite at ambient temperature, the fibre was pulled out to become longer and then closely combined with the matrix (Fig. 10a and b), indicating an obvious reinforcing role of the fibre. After a tensile fracture at 1500 °C, the cross-section of the composite was divided into oxidation and nonoxidation zones. The entire carbon fibre in the oxidation zone was eroded, leaving a hole, and the interface between the fibre and matrix was oxidized to form a glass phase. The nonoxidation zone is surrounded by the oxidation zone and is the main bearing area of composites at high temperatures, accounting for a small part of the entire composite, thereby degrading the overall tensile

Table 1 Bending and tensile strengths of C/C–SiC composites obtained by melting and siliconizing three types of preforms

Preform type	CVI/C	S/C	CVI/C + S/C
Density (g cm^{-3})	1.75	1.95	1.99
Porosity (%)	6.62%	21.29%	4.01%
Bending strength (MPa)	261.9	134.4	345.4
Tensile strength (MPa)	108.0	75.0	156.0

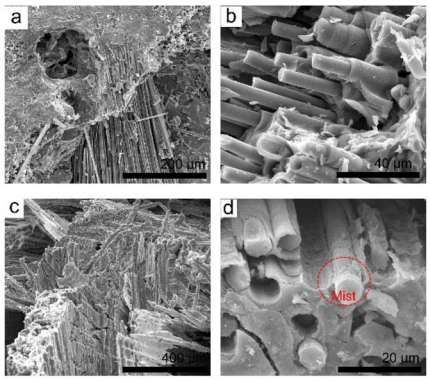

Fig. 10 Tensile fracture morphology of fibre composites: (a) and (b) ambient temperature; (c) and (d) 1500 °C.

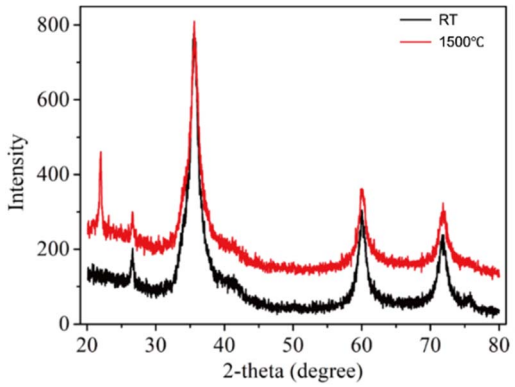

Fig. 11 XRD spectra of the C/SiC fibre composite after stretching at ambient temperature and 1500 °C.

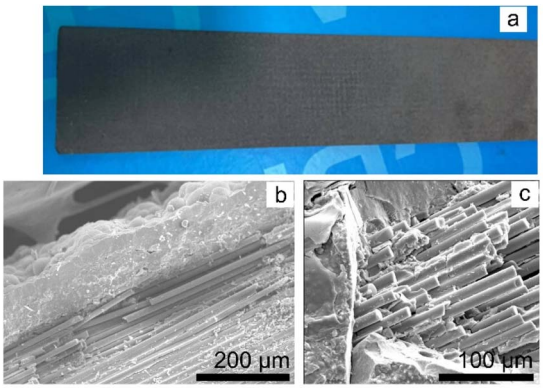

Fig. 12 (a) Photographs of coated fibre composites; (b) and (c) surface and cross-sectional morphologies of SiC coating, respectively.

properties of the composite. The phenomenon of fibre pull-out in the nonoxidized zone is obvious, and the fracture surface of the fibre shows obvious tensile characteristics. However, the fracture surface is covered with an oxide layer because the nonoxidized zone is also oxidized when exposed to air after the composite breaks.

According to the XRD patterns of the composites in Fig. 11, β-SiC diffraction peaks corresponding to the (111), (220), and (311) planes are observed in the composites at $2\theta = 36.5°$, 60.1°, and 71.9°, respectively, both at ambient temperature and under a 1500 °C air atmosphere. No obvious differences in the peak width and strength were observed under both temperature conditions, indicating that 1500 °C has no obvious influence on SiC. However, the C-peak (26.5°) intensity of the oxidized composite decreased significantly, and the diffraction peak of SiO_2 appeared at 20.9°. This is because the C fibre and PyC interface inside the material were consumed by oxidation; thus, the surface of the matrix began to be oxidized to produce SiO_2. With the sealing effect of SiO_2, some C fibres in the central area of the material were not severely oxidized. Both the C fibre and the SiC matrix of the C/SiC composites were oxidized at 1500 °C, which resulted in a rapid decline in the tensile strength of the materials.

3.4 Preparation and analysis of antioxidant coating performance

The C/SiC fibre composite sample was ultrasonically cleaned in deionized water, dried in a drying oven at 100 °C, and then placed in a chemical vapor furnace at 1200 °C to deposit a CVD-SiC oxidation-resistant coating on the composite surface. The image of the sample after deposition for 5 h is shown in Fig. 12a. Fig. 12b shows a surface SEM image of the SiC coating. The coating surface exhibits a cellular morphology of hemispherical particles composed of many fine grains. Fig. 12c shows the cross-sectional morphology of the coating sample. The coating is compact and flat, with a thickness of approximately 49 μm.

The tensile properties of C/C–SiC composites with CVD-SiC coatings at 1500 °C were also investigated. Fig. 13 shows the tensile load–displacement curve of the C/C–SiC composites with and without SiC coatings. The tensile strength of the C/SiC composite with a SiC coating is 107.87 MPa at 1500 °C, which is significantly higher than that of composites without SiC coatings, indicating that the SiC coating plays a role in oxidation resistance and heat insulation.

Fig. 14 compares the oxidation morphologies of uncoated and CVD SiC-coated C/C–SiC composites at 1500 °C. Uncoated composites exhibit severe oxidation degradation characterized by the following: substantial oxidation of both fibres and matrix; development of pronounced internal cracks; significant damage to the glass phase formed at fibre–matrix interfaces; complete fibre oxidation generating abundant pores; and distinct oxidation spots on the SiC matrix. This pervasive degradation causes drastic deterioration of tensile properties, as shown in Fig. 14a and b.

In contrast, SiC-coated composites (Fig. 14c and d) demonstrate enhanced carbon fibre retention – particularly in coating-proximal regions – though localized oxidation occurs in coating-distant zones where partial fibre consumption creates pores and enables significantly elongated fibre pull-out. Fracture

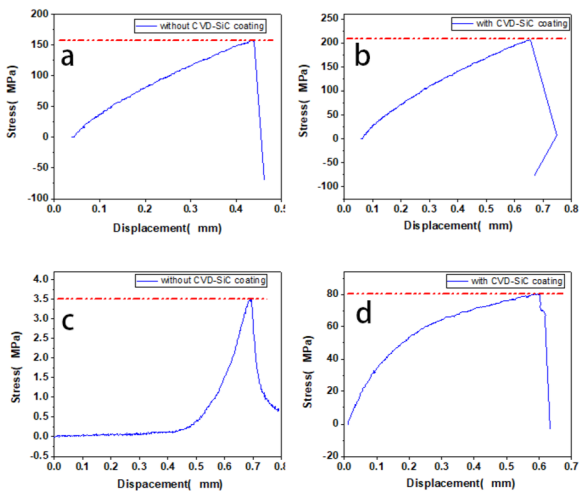

Fig. 13 Stress–displacement curves of C/C–SiC composites with and without CVD-SiC coating at ambient temperature (a & b) and 1500 °C (c & d).

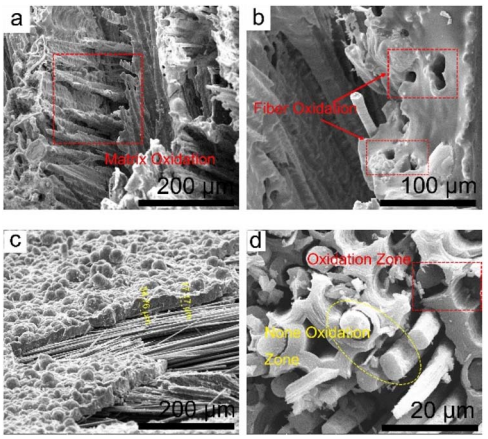

Fig. 14 Fracture morphology of the C/SiC fibre composite at 1500 °C: (a) and (b) without coating; (c) and (d) with coating.

surfaces show no extensive oxidation zones, featuring only partially oxidized exposed fibres.

Notably, the material's strength at 1500 °C shows a 50% reduction compared to room-temperature coated specimens.

Microstructures of C/C–SiC composites are an important factor that affects the oxidation. The crack defects generated during the preparation process provide channels for oxygen to penetrate the material. A key advantage of the RMI process in fabricating C/C–SiC composites lies in its high densification efficiency. Under capillary forces, molten silicon infiltrates minute pores and reacts with pre-infiltrated carbon. The resulting silicon carbide (SiC) occupies a slightly larger volume than the consumed carbon (molar volume: SiC ≈ 12.5 cm^3 mol^{-1}, C ≈ 5.3 cm^3 mol^{-1}), and this reaction contributes to further fill in the internal structure of the C/C–SiC composite.

As mentioned in the previous section, three methods were investigated for the preparation of carbon matrices, and alternating S/C and CVI-PyC was chosen as the optimal method. By using the optimal method, a more uniform distribution of carbon sources could be formed in the composite (as shown in the pore distribution diagram in Fig. 6). This facilitates complete silicon melt infiltration, resulting in the content of easily oxidizable carbon in the matrix being reduced, and the oxygen diffusion pathways are shortened. The resulting silicon carbide fills the pores, cracks, and fibre bundle gaps in the C/C preform, forming a continuously distributed ceramic matrix. This helps minimize channels for oxygen diffusion into the material and prolongs the path and time required for oxygen to reach the carbon fibres.

Besides the effect of microstructures on the oxidation resistance, there are some effects from the residual Si. Residual silicon, having a much lower melting point (~1414 °C) than SiC, solidifies last during cooling from RMI processing temperatures.[34,35] This can lead to the formation of relatively large, continuous pockets of silicon within the SiC matrix. A significant mismatch exists between the coefficient of thermal expansion of silicon and the surrounding phases, including SiC and carbon. This mismatch induces substantial residual stresses during cooling, which can lead to microcracking at the Si/SiC and Si/C interfaces. These silicon-rich regions and the associated weak, stressed interfaces act as preferential pathways for crack propagation. While strong interfaces and secondary phases can deflect cracks and increase toughness, the comparatively low strength and fracture toughness of silicon mean that cracks encountering a silicon pocket are more likely to propagate directly through it rather than being deflected. This results in a more direct, brittle fracture path, reducing the overall toughness of the composite. Although the residual Si is detrimental to the mechanical properties, it plays a crucial and largely beneficial role in the high-temperature oxidation performance of C/C–SiC composites.

4 Conclusions

The following conclusions were derived from this study:

(1) The phase composition of the C/C–SiC composites prepared through RMI comprises SiC, C, and residual Si. The porous C structure obtained after sucrose-derived carbon pyrolysis is more likely to react with Si, thereby producing SiC. However, after reacting with the infiltrated Si, the dense CVI-prepared PyC blocks the channel, making the complete reaction challenging. Therefore, after siliconizing CVI combined with S/C preforms, the residual Si phase is reduced and dispersed.

(2) The bending and tensile strengths of CVI-PyC and S/C after siliconizing are the highest (reaching 345.4 and 156 MPa, respectively), whereas the strength of sucrose-derived carbon after siliconizing is the lowest (reaching 134.4 and 75 MPa, respectively). The structure and morphology of C are the primary factors affecting the strength.

(3) CVD-SiC coating is critical for C/C–SiC fibre composites because it ensures the tensile strength of these composites at 1500 °C and exhibits good oxidation resistance, thereby ensuring their reliable aerospace applications.

Author contributions

YH and YC: idea for the article, literature search and analysis, experiment, writing and revision of the manuscript. SQ: literature search and experiment. HL and HL: idea for the article, analysis, revision of the manuscript. JM: revision of the manuscript. HS: experimental protocol design. XS: revision of the manuscript.

Conflicts of interest

There are no conflicts to declare.

Data availability

The authors confirm that the data supporting the findings of this study are available within the article.

Acknowledgements

The authors thank the support of the Key Project of the Joint Fund for Regional Innovation and Development, NSFC (No. U23A6014).

Notes and references

1 X. S. Zhang, L. W. Yang, H. T. Liu and M. Zu, A novel high-content CNT-reinforced SiC matrix composite-fiber by precursor infiltration and pyrolysis process, *RSC Adv.*, 2017, **7**, 23334–23341.

2 X. H. Li, Z. F. Xu, L. Chen, L. Hong and Y. Li, Thermal oxidation curing polycarbosilane fibers by alternating air and vacuum process, *RSC Adv.*, 2020, **10**, 26052–26058.

3 H. Shi, Q. Fu, B. Liu and F. Liu, Effect of porous pre-coating on the phase composition and oxidation protective performance of SiC coating by gaseous silicon infiltration, *Surf. Coat. Technol.*, 2024, **480**, 130597.

4 P. Kumar and V. K. Srivastava, Tribological behaviour of C/C–SiC composites—A review, *J. Adv. Ceram.*, 2016, **5**(1), 1–12.

5 W. Krenkel and F. Berndt, C/C–SiC composites for space applications and advanced friction systems, *Mater. Sci. Eng., A*, 2005, **412**(1), 177–181.

6 N. P. Bansal, *Handbook of Ceramic Composites*, Springer US, Boston, MA, 2005, pp. 117–148.

7 H. Sun, S. Fan, L. Wang, X. Ma, J. Deng, L. Cheng and L. Zhang, Microstructure and tribological properties of PIP-SiC modified C/C–SiC brake materials, *Ceram. Int.*, 2021, **47**(11), 15568–15579.

8 Z. Tang, M. Yi, Y. Zhou, R. Liu and K. Peng, Effect of high-temperature heat treatment on the microstructure and mechanical behavior of PIP-based C/C-SiC composites with SiC filler, *J. Eur. Ceram. Soc.*, 2021, **41**(15), 7610–7619.

9 S. Kumar, M. Bablu, A. Ranjan, L. Manocha and N. Prasad, Fabrication of 2D C/C-SiC composites using PIP based hybrid process and investigation of mechanical properties degradation under cyclic heating, *Ceram. Int.*, 2017, **43**(3), 3414–3423.

10 Y. R. Mahajan and R. Johnson, *Handbook of Advanced Ceramics and Composites: Defense, Security, Aerospace and Energy Applications*, Springer International Publishing, Cham, 2020, pp. 877–911.

11 L. Zhang, W. Wang, X. Gao, S. Li, K. Gui, G. Wang and R. He, Additive manufacturing of continuous carbon fibre reinforced high entropy ceramic matrix composites *via* paper laminating, direct slurry writing, and precursor infiltration and pyrolysis, *Ceram. Int.*, 2023, **49**(5), 7833–7841.

12 F. Servadei, L. Zoli, P. Galizia, C. Melandri and D. Scitiet, Preparation of UHTCMCs by hybrid processes coupling Polymer Infiltration and Pyrolysis with Hot Pressing and vice versa, *J. Eur. Ceram. Soc.*, 2022, **42**(5), 2118–2126.

13 Y. Ni, R. Luo and H. Luo, Fabrication and mechanical properties of 3-D Cf/C-SiC-TiC composites prepared by RMI, *J. Alloy Compd.*, 2019, **798**, 784–789.

14 Z. Xue, R. Xue, N. Zhang, L. Zhang, X. Liu, B. Hou, Y. Zhang and J. Wang, Water-Lubricated Friction Properties of C/C-SiC Composites with Different SiC-Phase Contents Fabricated by RMI, *Tribol. Trans.*, 2021, **64**(3), 468–476.

15 J. Wang, M. Lin, Z. Xu, Y. Zhang, Z. Shi, J. Qian, G. Qiao and Z. Jin, Microstructure and mechanical Microstructure and mechanical properties of C/C–SiC composites fabricated by a rapid processing method, *J. Eur. Ceram. Soc.*, 2009, **29**(14), 3091–3097.

16 C. Wang, Y. Liu, Q. You, F. Ye and L. Cheng, Effect of the pyrolytic carbon (PyC) content on the dielectric and electromagnetic interference shielding properties of layered SiC/PyC porous ceramics, *Ceram. Int.*, 2019, **45**(5), 5637–5647.

17 L. T. Jia, M. Q. Wang, X. F. Guo, J. Zhu, A. J. Li and Y. Q. Peng, Effect of chemical vapor infiltration on the flexural properties of C/C-SiC composites prepared by the precursor infiltration pyrolysis method, *New Carbon Mater.*, 2023, **38**(6), 1127–1134.

18 M. Wortmann, W. Keil, B. Brockhagen, J. Biedinger, M. Westphal, C. Weinberger, E. Diestelhorst, W. Hachmann, Y. Zhao, M. Tiemann, G. Reiss, B. Hüsgen, C. Schmidt, K. Sattler and N. Frese, Pyrolysis of sucrose-derived hydrochar, *J. Anal. Appl. Pyrolysis*, 2022, **161**, 105404.

19 I. F. Myronyuk, V. I. Mandzyuk, V. M. Sachko and V. M. Gun'ko, Structural Features of Carbons Produced Using Glucose, Lactose, and Saccharose, *Nanoscale Res. Lett.*, 2016, **11**(1), 508.

20 T. Guan, J. Zhao, G. Zhang, T. Guan, J. Zhao, G. Zhang, D. Zhang, B. Han, N. Tang, J. Wang and K. Li, Insight into controllability and predictability of pore structures in pitch-based activated carbons, *Microporous Mesoporous Mater.*, 2018, **271**, 118–127.

21 Q. Yan, X. Yang, X. Zhang, S. Wu, H. Li and Q. Huang, Effect of graphitization temperature on microstructure, mechanical and ablative properties of C/C composites with pitch and pyrocarbon dual-matrix, *Ceram. Int.*, 2023, **49**(2), 2860–2870.

22 W. Hong, X. Pang, H. Yan, L. Li and Z. Zhang, Actively-controlled PyC interphase failure mechanisms in C/SiC composite revealed using micro-mechanical interfacial testing, *Ceram. Int.*, 2025, **51**(3), 3654–3664.

23 Z. Zhang, M. Zhang, H. Duan, L. Li and Z. Zhang, PyC interphase growth mechanism and control models of C/SiC composites, *J. Eur. Ceram. Soc.*, 2023, **43**(14), 5961–5971.

24 Y. Q. Chen, H. B. He, C. Liu and X. H. Lu, Thermal decmposition of glucose and sucrose by kinetics analysi, *Chin. J. Process Eng.*, 2010, **10**(4), 720–725.

25 P. Körner P, D. Jung and A. Kruse, The effect of different Brønsted acids on the hydrothermal conversion of fructose to HMF, *Green Chem.*, 2018, **20**(10), 2231–2241.

26 H. Fang, Z. Sheng, W. Wang, C. Wei, S. Li, X. Geng, X. Li, N. Zhu, G. Wen, S. Dong and P. Wang, Formation and mechanism of carbon coating on carbon fibres through glucose-to-carbon conversion and its effect on the mechanical properties of Cf/ZrB_2-SiC composites, *J. Eur. Ceram. Soc.*, 2025, **45**(15), 117569.

27 I. C. Lewis, Chemistry of pitch carbonization, *Fuel*, 1987, **66**(11), 1527–1531.
28 L. P. Ran, Y. Q. Liu, L. Yang and M. Z. Yi, Effect of matrix carbon on properties of C/C-SiC composites fabricated by RMI, *Mater. Sci. Eng. Powder Met.*, 2011, **16**(03), 374–378.
29 R. Lin, R. Y. Luo and H. Luo, Effects of Density of C/C Preform and Reaction Temperature on the Mechanical Properties and Microstructure of C/C-SiC Composites, *Synthetic Mater. Aging Appl.*, 2018, **47**(01), 57–123.
30 G. Savage, *Gas Phase Impregnation/Densification of Carbon-Carbon and Other High-Temperature Composite Materials [M]//Carbon-Carbon Composites*, Springer Netherlands, Dordrecht, 1993, pp. 85–116.
31 A. Węgrzyniak, S. Jarcaewski, P. Kuśtrowski and P. Michorczyk, Influence of carbon precursor on porosity, surface composition and catalytic behaviour of CMK-3 in oxidative dehydrogenation of propane to propene, *J. Porous Mater.*, 2018, **25**(3), 687–696.
32 J. Yang and O. J. Ilegbusi, Kinetics of silicon–metal alloy infiltration into porous carbon, *Composites, Part A*, 2000, **31**(6), 617–625.
33 Q. Qin, Y. Han, Y. Zeng, M. Cai, S. Li, Z. Xiao, H. Xia and J. Wang, Microstructure and mechanical properties of 2D laminated C/C-SiC composites prepared by low-temperature reactive melt infiltration with silicon alloy, *J. Eur. Ceram. Soc.*, 2025, **45**(6), 117217.
34 F. Wan, T. J. Pirzada, R. Liu, Y. Wang, C. Zhang and T. M. Thomas, Microstructure Characterization by X-Ray Computed Tomography of C/C-SiC Ceramic Composites Fabricated with Different Carbon Fiber Architectures, *Appl. Compos. Mater.*, 2019, **26**(4), 1247–1260.
35 Y. Wei, Y. Wang, X. Xiong, Z. Ye and Z. Liu, Microstructure evolution and mechanical properties of C/C-SiC composites prepared with different prefabricated structures, *J. Mater. Eng.*, 2024, **52**(10), 127–138.